MIT Libraries | DSpace@MIT

MIT Open Access Articles

High Luminescence Efficiency in MoS

Massachusetts Institute of Technology

High Luminescence Efficiency in MoS2 Grown by Chemical Vapor Deposition

13 authors, including:

Robert A Burke
Pennsylvania State University
15 PUBLICATIONS   **264** CITATIONS

SEE PROFILE

Der-Hsien Lien
56 PUBLICATIONS   **1,512** CITATIONS

SEE PROFILE

Jing Kong
Massachusetts Institute of Technology
302 PUBLICATIONS   **17,834** CITATIONS

SEE PROFILE

Ali Javey
University of California, Berkeley
280 PUBLICATIONS   **21,346** CITATIONS

SEE PROFILE

Some of the authors of this publication are also working on these related projects:

Project 2D Materials View project

Project Hybrid PV/T Spectrum Splitting Collector View project

High Luminescence Efficiency in MoS$_2$ Grown by Chemical Vapor Deposition

Matin Amani,[†,‡] Robert A. Burke,[§] Xiang Ji,[∥] Peida Zhao,[†,‡] Der-Hsien Lien,[†,‡] Peyman Taheri,[†] Geun Ho Ahn,[†,‡] Daisuke Kirya,[†,‡] Joel W. Ager, III,[‡] Eli Yablonovitch,[†,‡] Jing Kong,[∥] Madan Dubey,[§] and Ali Javey*,[†,‡]

[†]Electrical Engineering and Computer Sciences, University of California at Berkeley, Berkeley, California 94720, United States

[‡]Materials Sciences Division, Lawrence Berkeley National Laboratory, Berkeley, California 94720, United States

[§]U.S. Army Research Laboratory, 2800 Powder Mill Road, Adelphi, Maryland 20783, United States

[∥]Electrical Engineering and Computer Sciences, Massachusetts Institute of Technology, 77 Mass Avenue, Cambridge, Massachusetts 02139, United States

S *Supporting Information*

ABSTRACT: One of the major challenges facing the rapidly growing field of two-dimensional (2D) transition metal dichalcogenides (TMDCs) is the development of growth techniques to enable large-area synthesis of high-quality materials. Chemical vapor deposition (CVD) is one of the leading techniques for the synthesis of TMDCs; however, the quality of the material produced is limited by defects formed during the growth process. A very useful nondestructive technique that can be utilized to probe defects in semiconductors is the room-temperature photoluminescence (PL) quantum yield (QY). It was recently demonstrated that a PL QY near 100% can be obtained in MoS$_2$ and WS$_2$ monolayers prepared by micromechanical exfoliation by treating samples with an organic superacid: bis(trifluoromethane)-sulfonimide (TFSI). Here we have performed a thorough exploration of this chemical treatment on CVD-grown MoS$_2$ samples. We find that

the as-grown monolayers must be transferred to a secondary substrate, which releases strain, to obtain high QY by TFSI treatment. Furthermore, we find that the sulfur precursor temperature during synthesis of the MoS$_2$ plays a critical role in the effectiveness of the treatment. By satisfying the aforementioned conditions we show that the PL QY of CVD-grown monolayers can be improved from ∼0.1% in the as-grown case to ∼30% after treatment, with enhancement factors ranging from 100 to 1500× depending on the initial monolayer quality. We also found that after TFSI treatment the PL emission from MoS$_2$ films was visible by eye despite the low absorption (5–10%). The discovery of an effective passivation strategy will speed the development of scalable high-performance optoelectronic and electronic devices based on MoS$_2$.

KEYWORDS: transition metal dichalcogenide, MoS$_2$, chemical vapor deposition, quantum yield, radiative lifetime, biexcitonic recombination
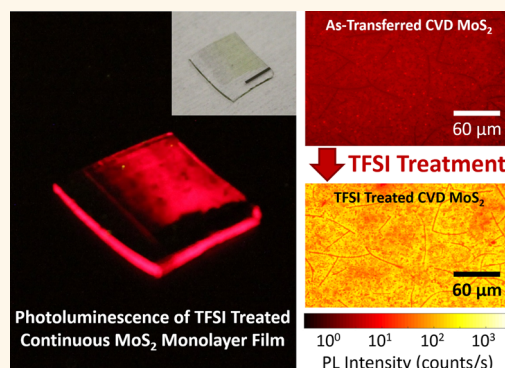
Two-dimensional (2D) materials, particularly transition metal dichalcogenides (TMDCs), have been the subject of a large amount of research interest over the past several years for both electronic and optoelectronic applications.[1,2] Unlike graphene, which is a semimetal at the monolayer limit,[3] TMDCs have direct optical band gaps in the range of 0.8 to 2.0 eV,[4–6] enabling their use as effective devices for both switching and light emission/detection. In addition, TMDCs can offer new functionalities over 3D semiconductors, such as their ability to form heterostructures free of lattice matching constraints[7] and tunable operation through the application of electric field and strain.[8,9] Valley and spin-based physics, which exist in monolayers of these materials, can also lead to a new classes of devices.[10,11] Tremendous progress

has been made in the growth of electronic quality graphene on the wafer scale[12] as well as roll-to-roll growth[13] for use as transparent conductors. More recently research groups have been investigating techniques to grow TMDC films.[14] Numerous research groups have demonstrated the growth of various TMDCs, including MoS$_2$, WS$_2$, and WSe$_2$.[15–17] However, a route to mitigate the effect of defects in these synthetic materials remains an issue facing the community.[18]

The ability to limit, passivate, or repair defects within synthetic TMDCs is a crucial prerequisite to the realization of high-performance devices. Electronic devices such as MOS-FETs, where the conduction mechanism is driven by majority carriers, are susceptible to defects. In MOSFETs, defects contribute to the interface states (D_{IT}), increasing the subthreshold swing.[19] In proposed technologies for sub-60 mV/decade switches, such as tunnel transistors, defects contribute to sub-band-gap states that result in a parasitic current pathway when the transistor is in the off-state, limiting the subthreshold swing and severely degrading the on/off ratio.[20] For optoelectronic devices where the operation is based on minority carriers, defects act as nonradiative recombination centers and result in fewer photons being emitted from the device than excited states generated through either optical or electrical pumping. Hence, defects in optoelectronic devices translate into a lowering of the efficiency for light-emitting diodes (LEDs) and an increase in the threshold current for solid-state lasers.[21]

The passivation of interfaces has been heavily investigated in all semiconductors. To realize high-performance silicon transistors, the Si/SiO_2 interface is annealed in forming gas. This allows hydrogen to passivate dangling bonds and results in an improved subthreshold swing and reduced hysteresis.[22] In GaAs, double-heterostructures (using an AlGaAs cladding layer) are utilized to create a virtual defect-free interface.[23,24] Similarly, interfacial passivation is a requirement for 2D materials, which is partially mediated due to the natural self-termination of the 2D lattice at the surface, resulting in no dangling bonds. However, the quality of the surface is still severely degraded by the presence of defects.[25] An effective way to evaluate semiconductor quality is to study the photo-luminescence (PL) quantum yield (QY), which is a ratio of the number of photons that a material emits compared to the number of photons absorbed.[23,26] Defects act as nonradiative recombination centers and significantly quench the emission. Previously, it was demonstrated that treatment using the organic superacid bis(trifluoromethane)sulfonamide (TFSI) resulted in a PL QY near 100% in exfoliated MoS_2 monolayers,[26] and it was later demonstrated that this treatment mechanism was also effective on exfoliated WS_2 monolayers.[27] A key unanswered question in these studies, however, is the effectiveness of the treatment on MoS_2 grown by chemical vapor deposition (CVD). We address treatment of synthetic MoS_2 monolayers in this work and show that tensile strain present in as-grown films[28] has a dramatic effect on the treatment. We also study the effect of the sulfur precursor temperature during growth and show that this also plays a role in the ultimate quantum yield, which can be achieved after treatment. As a result we are able to achieve large-area monolayers with high quantum yield.

RESULTS AND DISCUSSION

Figure 1b and c show schematic representations of the two approaches investigated to obtain high QY synthetic MoS_2 monolayers. Samples that were grown and treated directly by TFSI (Figure 1b) had a minimal change in the QY with peak values under 0.1%. In the second approach (Figure 1c), the MoS_2 triangular domains and films were transferred from the growth substrate to a new substrate using HF to release MoS_2 from the original substrate. It has been previously shown that after CVD growth there is an intrinsic tensile strain present in MoS_2 monolayers,[28,31] which may be a result of the difference
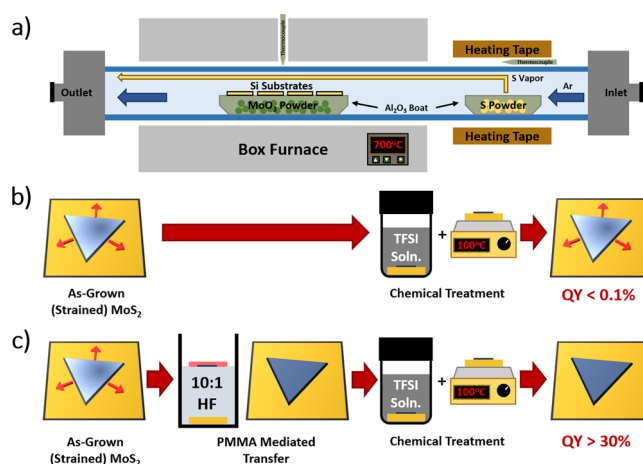

Figure 1. (a) Configuration of the growth setup utilized to prepare the MoS_2 samples for this study. The temperature of the substrate and molybdenum precursor (in the furnace hot zone) and the sulfur precursor (surrounded by heating tape) is controlled and measured independently. (b and c) Schematic illustrating the two primary sample preparation routes investigated in this study. As-grown MoS_2 triangular domains and films, which show tensile strain after growth were either (b) treated by TFSI directly, resulting in a small reduction in the PL QY, or (c) transferred from the growth substrate using a PMMA-mediated transfer process, releasing the strain, and subsequently treated by TFSI, resulting in a final PL QY of approximately 30%.

in thermal expansion coefficient of the Si/SiO_2 substrate and MoS_2 as the sample is cooled from the growth temperature (typically in the range 600−800 °C) to room temperature. After the layer transfer, the strain is released, and the samples are subsequently treated by TFSI, resulting in a dramatic enhancement of the room temperature quantum yield from <1% before treatment to a final value of ∼30%.

Influence of Layer Transfer on the Optoelectronic Properties. We first investigated the effect of layer transfer on the optoelectronic properties of MoS_2. For this study single MoS_2 domains were grown directly on quartz substrates and subsequently transferred to a new quartz substrate as described in section 2.1. Consistent with previous reports, we find that there is intrinsic biaxial tensile strain in the as-grown MoS_2 domains as a result of the difference in the thermal expansion coefficient of the substrate and the MoS_2.[28,31] As a result, we observe a shift of the in-plane Raman mode (E′) of 2.4 cm^{-1} between the as-grown and transferred films, indicating that the as-grown MoS_2 is under 0.8% tensile strain (Figure 2a). The final separation of the E′ and A′ peaks is 18.5 cm^{-1} after transfer, which is consistent with what has been previously reported for monolayer MoS_2 produced by exfoliation.[28] We also observe a blue-shift of the PL spectra, which similarly corresponds to a release of tensile strain as shown in Figure 2b.

The dependence of the PL QY as a function of pump power was then investigated both before and after transfer over a pump dynamic range of 5 orders of magnitude, as shown in Figure 2c, where the limits were set by either insufficient signal due to the low QY of the untreated samples or high illumination powers (greater than 100 μW), which can damage the monolayers due to excessive local heating. The corresponding QY as a function of pump power is plotted in Figure 2d and shows that the quantum yield for the CVD samples prepared here is in the range of 0.02% to 0.5%. Interestingly, the dynamics of the PL QY as a function of pump power change
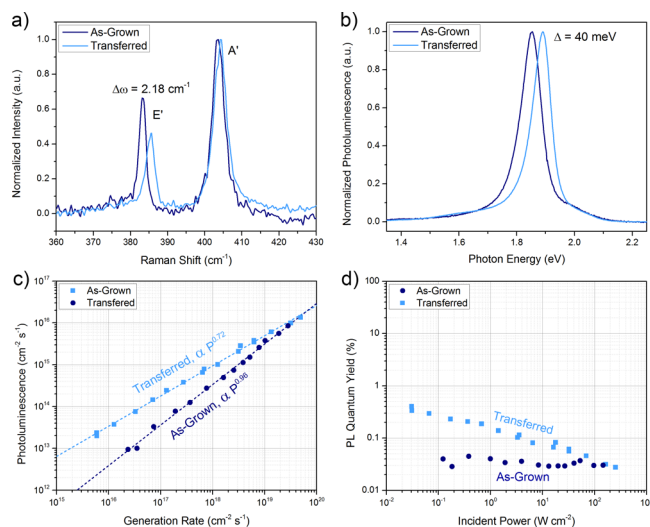
Figure 2. (a) Raman spectra measured on as-grown and transferred MoS$_2$ single domains. (b) PL spectra of the MoS$_2$ single domains measured before and after transfer at a laser power of 50 W/cm^2. (c) Pump-power dependence of the integrated PL measured before and after transfer. Dashed lines show power law fits of the data. (d) Pump-power dependence of the QY measured before and after transfer. Samples shown here were grown directly on quartz and subsequently transferred to a new quartz substrate.

Figure 3. (a) Pump-power dependence of the QY measured on a CVD-grown MoS$_2$ single domain after growth and after chemical treatment by TFSI. Note that this sample was not transferred. (b) Pump-power dependence of the QY measured on a CVD-grown MoS$_2$ single domain after transfer and after chemical treatment by TFSI. Dashed lines show the recombination model for the treated sample.

dramatically after the strain is released, as can be seen by the difference in the power law dependence for the two samples. For the transferred sample, the behavior closely matches data that have been previously reported for exfoliated films, obeying a power law of 0.72 over the measurable dynamic range (Figure 2c). On the other hand, for the as-grown MoS$_2$ domains, the emission is linearly dependent on the incident power, with a power law of 0.98. In the unstrained case, monolayer MoS$_2$ shows a direct band gap at the K point; however, upon introduction of tensile strain (on the order of 1%) it has been previously calculated that the lowest energy transition becomes K-to-Γ and is indirect.[32]

The primary implication of having an indirect as opposed to direct band gap in semiconductors is the requirement of a phonon to observe a radiative transition. This additional requirement results in a dramatic increase in the radiative lifetime. In the case of direct band gap GaAs, the radiative lifetime is on the order of nanoseconds, while in indirect band gap silicon the radiative lifetime is on the order of milliseconds.[33,34] It is important to note here that an indirect band gap does not imply that a material has no luminescence. In fact, high-quality silicon with appropriate surface passivation can have a PL QY as high as 20%.[35] The indirect band gap simply implies that the nonradiative lifetime must be sufficiently long (ideally much longer than the radiative lifetime) to allow carriers the opportunity to radiate. It is likely that the tensile strain present in the as-grown MoS$_2$ leads to the material becoming more indirect, increasing the radiative lifetime and resulting in the observed variation in the pump-power dependence of the luminescence.

Chemical Treatment of as-Grown and as-Transferred MoS$_2$. The effects of chemical treatment on both as-grown and -transferred samples is studied by calibrated PL measurements. For as-grown MoS$_2$ monolayers, treatment by TFSI surprisingly leads to a minor degradation of the luminescence (Figure 3a). This behavior was consistently observed for numerous samples,
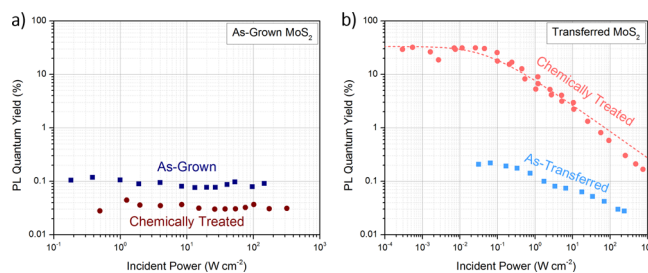
and similar results were observed for samples where the growth conditions were varied as discussed later. Noticeably different behavior was observed after the samples were transferred, as shown in Figure 3b. After transfer, samples grown at an optimized sulfur precursor temperature of 200 °C were found to have an average QY value of 31 ± 8% with TFSI treatment at low pump power. Similar pump-power dependence of PL QY was observed for a transferred MoS$_2$ continuous film after treatment by TFSI and is shown in Figure S5.

We can effectively model the luminescence of the chemically treated CVD MoS$_2$ using the previously proposed kinetic model, which is discussed in detail in refs 26 and 27. Recombination processes in most semiconductors are based on free carriers; however, this cannot be applied to 2D semiconductors, since they possess large exciton binding energies on the order of 200−500 meV.[36,37] In the excitonic model, generated free carriers can either recombine non-radiatively at defect sites or nonreversibly form excitons. The resulting excitons can then radiatively recombine, emitting light, or recombine nonradiatively with a second exciton (biexcitonic recombination), which is a similar process to Auger recombination in free carrier-based systems. The final form of the quantum yield is expressed as

$$QY = \frac{\tau_r^{-1}\langle N \rangle}{\tau_r^{-1}\langle N \rangle + B_{nr}n^2 + C_{bx}\langle N \rangle^2}$$

where n is the electron concentration (and is equal to the hole concentration for an optically pumped semiconductor with low background doping), $\langle N \rangle$ is the exciton concentration, τ_r is the radiative lifetime, B_{nr} is the defect mediated recombination rate, and C_{bx} is the biexcitonic recombination rate. To model the recombination in treated CVD MoS$_2$ samples transferred to quartz, we utilize the same radiative lifetime (10.8 ns) and biexcitonic recombination coefficient (2.8 cm^2 s^{-1}) extracted for exfoliated samples after chemical treatment.[26] However, since these samples do not show an ideal QY at low excitation power, the defect-mediated recombination rate, B_{nr}, is increased to 2 × 10^4 cm^2 s^{-1}. For comparison this value is approximately 2 orders of magnitude lower than what was previously calculated for as-exfoliated MoS$_2$ (untreated).

To verify that the structural properties of the CVD-grown MoS$_2$ are unaffected due to the TFSI treatment, we performed Raman spectroscopy before and after treatment as shown in Figure 4a and verify that, similar to the case of exfoliated monolayers, there is no significant change in the spectra.[26] PL
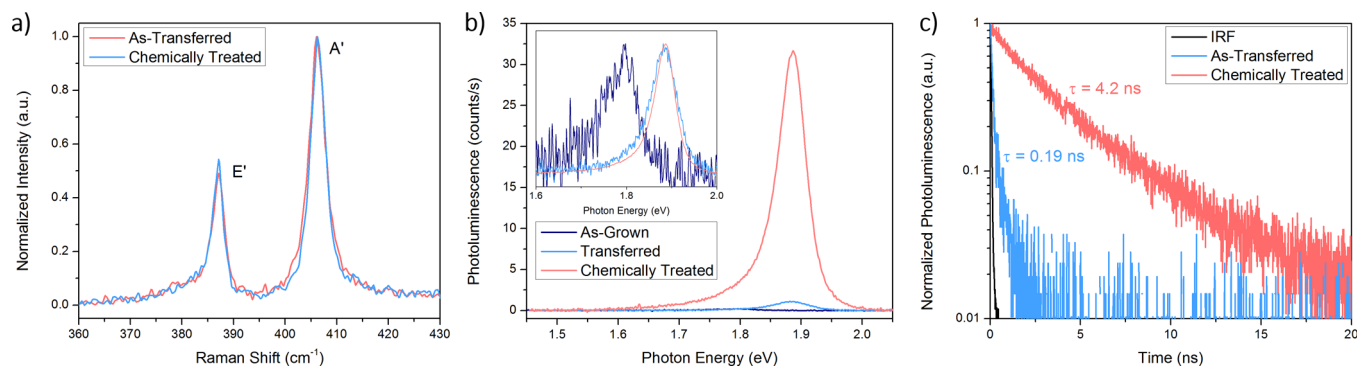
Figure 4. (a) Raman spectra measured on transferred MoS_2 single domains before and after treatment by TFSI. (b) PL spectra obtained at a pump power of 0.1 W/cm^2 for transferred MoS_2 single domains both before and after chemical treatment by TFSI. (c) Radiative decay of transferred MoS_2 single domains obtained at a pump fluence of 5×10^{-2} μJ/cm^2 both before and after chemical treatment by TFSI, as well as the instrument response function (IRF).

spectra measured after growth, transfer, and treatment at an incident power of 0.1 W/cm^2 are shown in Figure 4b. Noting that the significant spectral shift between the as-grown and transferred sample is a result of strain, we see no significant change in the spectral shape or peak position as a result of the treatment. It is also important to note that we do not observe any change in the spectral shape of the emission over the full pump dynamic range for treated samples, as shown in Figure S6. Finally, to confirm the enhancement in QY by chemical treatment, we performed time-resolved measurements at a low pump fluence of 5×10^{-2} μJ/cm^2. Prior to treatment, the films show an extremely short lifetime of 190 ps, which is comparable to the instrument timing resolution. After treatment, we observe a measured lifetime (τ_m) of 4.2 ns. We can estimate the quantum yield using the formula

$$QY = \frac{\tau_m}{\tau_r}$$

and the radiative lifetime measured in an exfoliated MoS_2 sample.[26] This results in a predicted quantum yield value of 38% and is in reasonable agreement with the steady-state measurements.

Effect of Sulfur Temperature on the Effectiveness of the Treatment. While the defects in MoS_2 monolayers generated by micromechanical exfoliation primarily consist of sulfur vacancies,[38−40] TEM studies have shown that samples grown by CVD contain a wide variety of complex defects.[25] These include point defects such a Mo or S antisites, Mo vacancies, sulfur and disulfur vacancies, Mo and S adatoms, and complexes such as ring chains.[25] To obtain MoS_2 samples where the TFSI treatment, which has previously been shown to be successful in passivating exfoliated monolayers, is effective, we studied the influence of sulfur precursor temperature on the growth. Figure 5 shows the quantum yield for each condition after transfer as well as after chemical treatment by TFSI for sulfur precursor temperatures of 200, 250, and 300 °C. For samples grown in sulfur-rich conditions, TFSI treatment had little impact on the quantum yield. Conversely, for samples prepared in sulfur-deficient conditions, a large enhancement of the PL was observed after treatment. We hypothesize that under sulfur-deficient growth conditions the defects in the sample are dominated by sulfur vacancies, making them more amenable to TFSI treatment, whereas in sulfur-rich conditions, the defects are primarily related to the cation and cannot be passivated by TFSI. Since the mechanism of TFSI treatment is
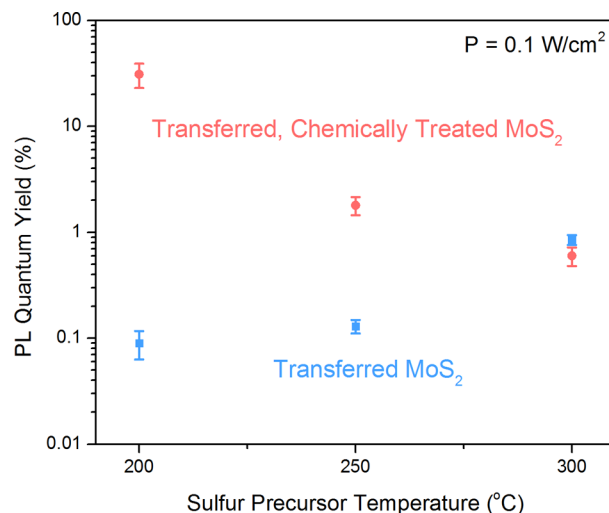

Figure 5. Maximum quantum yield obtained on CVD-grown single domains after transfer and after subsequent treatment by TFSI as a function of the sulfur precursor temperature during the growth process. Error bars are obtained from measurements taken on 10 different locations on the same sample.

not fully understood, however, we lack sufficient evidence to make a stronger claim based on these results. Interestingly, we found that in the absence of chemical treatment MoS_2 prepared in sulfur-rich conditions shows the highest emission efficiency.

Luminescence Uniformity. The uniformity of the transferred samples both before and after treatment was investigated using PL imaging. Emission from both single MoS_2 domains as well as continuous films was imaged, and the results are shown in Figure 6. As a result of the transfer process, some local imperfections such as holes are generated in the samples. Additionally, since the growth process has not been optimized yet at low sulfur pressure conditions, regions of few-layered growth and overgrowth along boundary regions of the films are observed. For both films and single domains, we observed uniform enhancement of the luminescence, excluding regions where the sample was physically damaged prior to treatment and multilayer regions in the continuous film. This is in strong contrast to previous observations in CVD samples where groups have reported the observation of high PL confined to edges or other local regions of the film.[41]

Finally, we performed macroscale imaging of the luminescence from the previously examined CVD MoS_2 film after
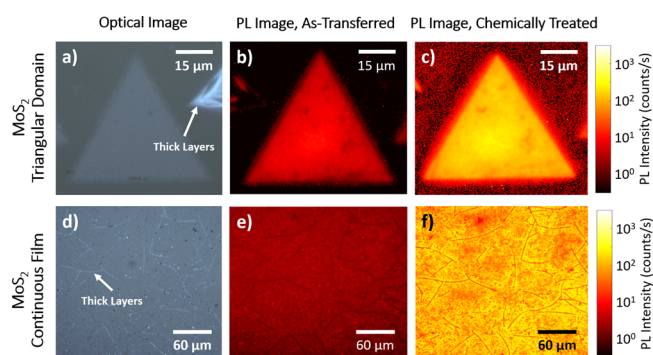
Figure 6. (a) Optical image of a transferred MoS$_2$ single domain and log-scale luminescence images from the same area obtained (b) before and (c) after chemical treatment by TFSI. (d) Optical image of a transferred continuous MoS$_2$ film and log scale luminescence images from the same area obtained (e) before and (f) after chemical treatment by TFSI.

chemical treatment by TFSI, and the results are shown in Figure 7. The image was taken by a photographic camera, using
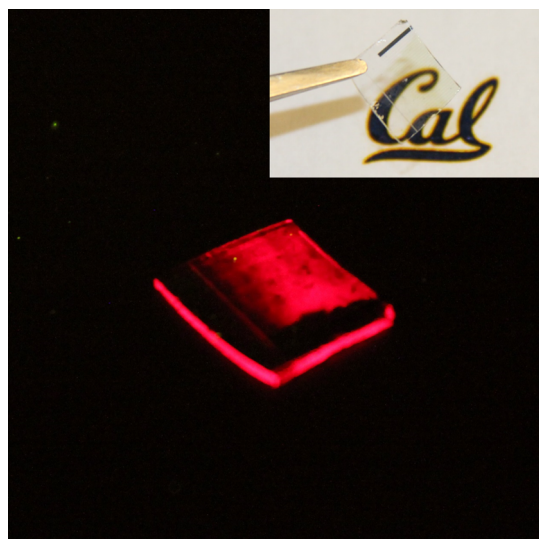

Figure 7. Photograph of luminescence from a CVD-grown MoS$_2$ film transferred to a quartz substrate and subsequently chemically treated by TFSI. The MoS$_2$ film partially covers the sample. Inset shows a photograph of the quartz chip and the transferred MoS$_2$ film.

a colored glass filter to block the excitation, and the sample was excited by an ultraviolet LED ($P \approx 0.2$ W/cm^2). Emission observed at the edges of the sample is due to light trapping within the high refractive index substrate. The strong, visible light emission of these monolayers coupled with their low absorption suggests that they have potential for use in transparent lighting applications.

CONCLUSION

In conclusion, we have demonstrated that treatment by TFSI can provide a highly effective and simple route to obtaining high luminescence efficiency in synthetic MoS$_2$. We have identified two key sample requirements for this treatment to be effective: (1) transfer of the MoS$_2$ film to release tensile strain of the as-grown films and (2) optimization of the sulfur precursor temperature during growth. As a result of the TFSI

treatment, we obtain CVD-grown MoS$_2$ samples with high PL QY values around 30%. Upon TFSI treatment, the monolayer MoS$_2$ film grown by CVD is shown to have visible-by-eye luminescence over a large area, despite having a low absorption coefficient. These findings provide important insight into the realization of a synthetic route toward high-quality monolayer TMDCs with low trap densities.

METHODS

MoS$_2$ Growth and Transfer. Monolayer MoS$_2$ triangular domains and films were grown, on either quartz or SiO$_2$/Si substrates, by atmospheric pressure CVD. Prior to growth, the substrates were cleaned in a piranha solution for 15 min followed by a 5 min soak in dionized (DI) water, acetone, and isopropyl alcohol. Afterward, 40 μL of perylene-3,4,9,10-tetracarboxylic acid tetrapotassium salt (PTAS) was spin coated on each sample as a seeding layer for the growth. A schematic of the CVD furnace used to grow the films is shown in Figure 1a. The sulfur precursor (15−33 mg) was loaded in an alumina boat and placed in a region outside of the furnace, where the temperature could be controlled by a heating tape. The sulfur precursor temperature was varied from 200 to 300 °C to grow the various triangular domains and films investigated in this study. MoO$_3$ powder (18−20 mg) was added to a second alumina boat, and four PTAS-coated substrates were placed on top of the alumina boat facing up. This boat was loaded into the center of the furnace for growth. The growth process was performed in a tube furnace at a sample temperature of 700 °C for growth involving SiO$_2$/Si substrates and 750 °C for quartz. The growth was carried out for 10 min, during which argon (5 sccm) was used as a carrier gas. An argon flow rate of 200 sccm was used before the growth to purge the tube and after to quench the growth process. Optical images of the resulting as-grown MoS$_2$ triangles and film regions are shown in Figures S1 and S2.

The resulting MoS$_2$ was transferred from the original growth substrate to a quartz substrate using poly(methyl methacrylate) (PMMA)-mediated transfer. A film of 495 PMMA A11 was spun onto the samples and was allowed to dry in air overnight. The PMMA at the edges of the samples was then removed, and the samples were placed in diluted hydrofluoric acid (10:1) to etch the oxide. After the substrate was either etched or released (the total etch time varied from 1 to 10 h), the PMMA/MoS$_2$ film was placed in several subsequent water baths and was ultimately transferred to the final quartz substrate. The film was allowed to dry for 12 h, and then the PMMA was removed in hot acetone and the substrate was rinsed with isopropyl alcohol.

Chemical Treatment. Samples were treated using a procedure similar to what was described in our previous work.[26] A 20 mg amount of TFSI (Sigma-Aldrich) was dissolved in 10 mL of acetonitrile to make a 2 mg/mL solution. Immediately prior to treatment, the samples were annealed at 300 °C for 2 h in a forming gas environment. The CVD samples were then immersed in the 2 mg/mL solution in a tightly capped vial at room temperature for 10 min. The samples were then removed, blow dried with nitrogen gas without rinsing, and annealed on a hot plate at 100 °C for 5 min. We found that the treatment using our previously reported conditions for exfoliated samples, i.e., 0.2 mg/mL TFSI in a 9:1 mixture of 1,2-dichlorobenzene and 1,2-dichloroethane at 100 °C, still resulted in significant enhancement of the PL QY (Figure S3) but was less effective on CVD samples than TFSI in acetonitrile. Treatment of both exfoliated and CVD films in acetonitrile was used as a control experiment to determine the effect of the solvent and resulted in minimal change in the PL (Figure S4).

Optical Characterization. The PL data presented in this work were obtained using the same custom-built micro-PL instrument described in our previous study.[26] In brief, steady-state measurements were performed using the 514.5 nm line of an Ar$^+$ laser (Lexel 95), and the laser power was adjusted using neutral density filters. In order to enable measurements at low (<50 nW) excitations, the system was designed such that the incident power on the sample was ∼130× less than the sampled laser power, which is measured during the PL

integration. For measurements taken at laser powers greater than 500 pW on the sample, the power was measured using a power meter (ThorLabs S120C). When the incident laser power was below 500 pW, lock-in detection from the output of a calibrated photodiode was used. All values were cross-calibrated at multiple laser powers to ensure that the photon flux on the sample was accurately known. The laser was focused on the sample using an 80× objective lens (NA = 0.9). The PL signal was collected using the same objective lens, passed through a 550 nm dielectric long-pass filter, dispersed by an $f = 340$ mm spectrometer with a 150 g/mm grating, and detected using a Si CCD camera (Andor iDus BEX2-DD). Prior to each measurement, the CCD background was obtained and subsequently subtracted from the PL acquisition. The sensitivity of the instrument as a function of wavelength (instrument function) was determined through measurement of a virtual Lambertian blackbody source under the objective, created by imaging the illumination from a temperature-stabilized lamp (ThorLabs SLS201) on a diffuse reflector (Spectralon). The system efficiency was determined by measuring the response of the excitation laser focused onto a diffuse reflector (Spectralon) with the 550 nm long-pass filter removed. The measured external quantum efficiency was converted to QY using the sample absorption at the pump wavelength and the fraction of light that is able to escape the sample ($1/4n^2$, where n is the refractive index of the medium[29]). For samples measured on Si/SiO$_2$ substrates (not transferred), the external quantum efficiency was also corrected for using a previously reported multiple reflection model.[30]

Time-resolved measurements were performed using pulsed light at 10 MHz generated by a supercontinuum laser (Fianium WhiteLase SC-400). A wavelength of 514 nm was selected using a double monochromator and focused on the sample using an 80× objective lens (NA = 0.9). An avalanche photodiode operating in single photon counting mode (IDQuantiqe) was used as the detector, and the signal was analyzed using a time-correlated single photon counting module (Becker-Hickl GmbH). PL imaging was performed on the samples in order to determine their uniformity. Measurements were performed using a florescence microscopy setup using a 470 nm LED as the excitation source and a CCD detector (Andor Luca). The photograph of luminesce from a full chip was taken using a 420 nm LED as the excitation source, which was passed through a diffuser and a collimating lens. The approximate power density at the sample plane was ~0.2 W/cm^2. The PL was detected using a Canon T1i EOS camera with a 58 mm lens (f/5.6) and an exposure time of 1/10 s. A 530 nm colored glass long-pass filter was used to block the excitation signal. Raman measurements were performed to determine the strain in the as-grown MoS$_2$ monolayer samples as well as to confirm that the strain was released upon transfer to a new substrate. Raman spectra were obtained using a Horiba LabRAM HR800 spectrometer in the backscattering geometry using a 532 nm laser focused through a 100× objective for excitation and collection.

ASSOCIATED CONTENT

Ⓢ Supporting Information

The Supporting Information is available free of charge on the ACS Publications website at DOI: 10.1021/acsnano.6b03443.

> Additional optical microscope images of CVD samples, pump-power dependence of PL QY on additional samples, control measurements of exfoliated and CVD MoS$_2$ treated in acetonitrile (no TFSI), and normalized PL spectra of a treated CVD sample as a function of pump power (PDF)

AUTHOR INFORMATION

Corresponding Author

*E-mail (A. Javey): ajavey@berkeley.edu.

Notes

The authors declare no competing financial interest.

REFERENCES

(1) Wu, S.; Buckley, S.; Schaibley, J. R.; Feng, L.; Yan, J.; Mandrus, D. G.; Hatami, F.; Yao, W.; Vuckovic, J.; Majumdar, A.; Xu, X. Monolayer Semiconductor Nanocavity Lasers with Ultralow Thresholds. *Nature* **2015**, *520*, 69−72.

(2) Sarkar, D.; Xie, X.; Liu, W.; Cao, W.; Kang, J.; Gong, Y.; Kraemer, S.; Ajayan, P. M.; Banerjee, K. A Subthermionic Tunnel Field-Effect Transistor with an Atomically Thin Channel. *Nature* **2015**, *526*, 91−95.

(3) Geim, A. K.; Novoselov, K. S. The rise of graphene. *Nat. Mater.* **2007**, *6*, 183−191.

(4) Splendiani, A.; Sun, L.; Zhang, Y.; Li, T.; Kim, J.; Chim, C.-Y.; Galli, G.; Wang, F. Emerging Photoluminescence in Monolayer MoS$_2$. *Nano Lett.* **2010**, *10*, 1271−1275.

(5) Zhao, W.; Ghorannevis, Z.; Chu, L.; Toh, M.; Kloc, C.; Tan, P.-H.; Eda, G. Evolution of Electronic Structure in Atomically Thin Sheets of WS$_2$ and WSe$_2$. *ACS Nano* **2013**, *7*, 791−797.

(6) Ruppert, C.; Aslan, O. B.; Heinz, T. F. Optical Properties and Band Gap of Single- and Few-Layer MoTe$_2$ Crystals. *Nano Lett.* **2014**, *14*, 6231−6236.

(7) Fang, H.; Battagli, C.; Carraro, C.; Nemsak, S.; Ozdol, B.; Kang, J. S.; Bechtel, H. A.; Desai, S. B.; Kronast, F.; Unal, A. A.; Conti, G.; Conlon, C.; Palsson, G. K.; Martin, M. C.; Minor, A. M.; Fadley, C. S.; Yablonovitch, E.; Maboudian, R.; Javey, A. Strong Interlayer Coupling in Van der Waals heterostructures Built from Single-Layer Chalcogenides. *Proc. Natl. Acad. Sci. U. S. A.* **2014**, *111*, 6198−6202.

(8) Ramasubramaniam, A.; Naveh, D.; Towe, E. Tunable Band Gaps in Bilayer Transition-Metal Dichalcogenides. *Phys. Rev. B: Condens. Matter Mater. Phys.* **2011**, *84*, 205325.

(9) McCreary, A.; Ghosh, R.; Amani, M.; Wang, J.; Duerloo, K.-A. N.; Sharma, A.; Jarvis, K.; Reed, E. J.; Dongare, A. M.; Banerjee, S. K.; Terrones, M.; Namburu, R. R.; Dubey, M. Effects of Uniaxial and Biaxial Strain on Few-Layered Terrace Structures of MoS$_2$ Grown by Vapor Transport. *ACS Nano* **2016**, *10*, 3186−3197.

(10) Xiao, D.; Liu, G. B.; Feng, W.; Xu, X.; Yao, W. Coupled Spin and Valley Physics in Monolayers of MoS$_2$ and Other Group-VI Dichalcogenides. *Phys. Rev. Lett.* **2012**, *108*, 196802.

(11) Zeng, H.; Dai, J.; Yao, W.; Xiao, D.; Cui, X. Valley Polarization in MoS$_2$ Monolayers by Optical Pumping. *Nat. Nanotechnol.* **2012**, *7*, 490−493.

(12) Lee, J.-H.; Lee, E. K.; Joo, W.-J.; Jang, Y.; Kim, B.-S.; Lim, J. Y.; Choi, S.-H.; Ahn, S. J.; Ahn, J. J.; Park, M.-H.; Yang, C.-W.; Choi, B. L.; Hwang, S.-W.; Whang, D. Wafer-Scale Growth of Single-Crystal Monolayer Graphene on Reusable Hydrogen-Terminated Germanium. *Science* **2014**, *344*, 286−289.

(13) Bae, S.; Kim, H.; Lee, Y.; Xu, X.; Park, J.-S.; Zheng, Y.; Balakrishnan, J.; Lei, T.; Kim, H. R.; Song, Y. I.; Kim, Y.-J.; Kim, K. S.; Ozyilmaz, B.; Ahn, J.-H.; Hong, B. H.; Iijima, S. Roll-to-Roll Production of 30-Inch Graphene Films for Transparent Electrodes. *Nat. Nanotechnol.* **2010**, *5*, 574−578.

(14) Najmaei, S.; Liu, Z.; Zhou, W.; Zou, X.; Shi, G.; Lei, S.; Yakobson, B. I.; Idrobo, J.-C.; Ajayan, P. M.; Lou, J. Vapour Phase Growth and Grain Boundary Structure of Molybdenum Disulphide Atomic Layers. *Nat. Mater.* **2013**, *12*, 754−759.

(15) Ling, X.; Lee, Y.-H.; Lin, Y.; Fang, W.; Yu, L.; Dresselhaus, M. S.; Kong, J. Role of the Seeding Promoter in MoS_2 Growth by Chemical Vapor Deposition. *Nano Lett.* **2014**, *14*, 464−472.

(16) Zhou, H.; Wang, C.; Shaw, J. C.; Cheng, R.; Chen, Y.; Huang, X.; Liu, Y.; Weiss, N. O.; Lin, Z.; Huang, Y.; Duan, X. Large Area Growth and Electrical Properties of p-Type WSe_2 Atomic Layers. *Nano Lett.* **2015**, *15*, 709−713.

(17) Kang, K.; Xie, S.; Huang, L.; Han, Y.; Huang, P. Y.; Mak, K. F.; Kim, C.-J.; Muller, D.; Park, J. High-Mobility Three-Atom-Thick Semiconducting Films with Wafer-Scale Homogeneity. *Nature* **2015**, *520*, 656−660.

(18) Wang, Q. H.; Kalantar-Zadeh, K.; Kis, A.; Coleman, J. N.; Strano, M. S. Electronics and Optoelectronics of Two-Dimensional Transition Metal Dichalcogenides. *Nat. Nanotechnol.* **2012**, *7*, 699−712.

(19) Martens, K.; Chui, C. O.; Brammertz, G.; Jaeger, B. D.; Kuzum, D.; Meuris, M.; Heyns, M. M.; Krishnamohan, T.; Saraswat, K.; Maes, H. E.; Groeseneken, G. On the Correct Extraction of Interface Trap Density of MOS Devices with High-Mobility Semiconductor Substrates. *IEEE Trans. Electron Devices* **2008**, *55*, 547−556.

(20) Ionescu, A. M.; Riel, H. Tunnel Field-Effect Transistors as Energy-Efficient Electronic Switches. *Nature* **2011**, *479*, 329−337.

(21) Ye, Y.; Wong, Z. J.; Lu, X.; Ni, X.; Zhu, H.; Chen, X.; Wang, Y.; Zhang, X. Monolayer Excitonic Laser. *Nat. Photonics* **2015**, *9*, 733−737.

(22) Reed, M. L.; Plummer, J. D. Chemistry of Si-SiO_2 Interface Trap Annealing. *J. Appl. Phys.* **1988**, *63*, 5776−5793.

(23) Schnitzer, I.; Yablonovitch, E.; Caneau, C.; Gmitter, T. J. Ultrahigh Spontaneous Emission Quantum Efficiency, 99.7% Internally and 72% Externally, from AlGaAs/GaAs/AlGaAs Double Heterostructures. *Appl. Phys. Lett.* **1993**, *62*, 131−133.

(24) Guidotti, D.; Hasan, E.; Hovel, H. J.; Albert, M. Degradation of Band-Gap Photoluminescence in GaAs. *Appl. Phys. Lett.* **1987**, *50*, 912−914.

(25) Zhou, W.; Zou, X.; Najmaei, S.; Liu, Z.; Shi, Y.; Kong, J.; Lou, J.; Ajayan, P. M.; Yakobson, B. I.; Idrobo, J.-C. Intrinsic Structural Defects in Monolayer Molybdenum Disulfide. *Nano Lett.* **2013**, *13*, 2615−2622.

(26) Amani, M.; Lien, D.-H.; Kiriya, D.; Xiao, J.; Azcatl, A.; Noh, J.; Madhvapathy, S. R.; Addou, R.; Kc, S.; Dubey, M.; Cho, K.; Wallace, R. M.; Lee, S.-C.; He, J.-H.; Ager, J. W.; Zhang, X.; Yablonovitch, E.; Javey, A. Near-Unity Photoluminescence Quantum Yield in MoS2. *Science* **2015**, *350*, 1065−1068.

(27) Amani, M.; Taheri, P.; Addou, R.; Ahn, G. H.; Kiriya, D.; Lien, D.-H.; Ager, J. W.; Wallace, R. M.; Javey, A. Recombination Kinetics and Effects of Superacid Treatment in Sulfur- and Selenium Based Transition Metal Dichalcogenides. *Nano Lett.* **2016**, *16*, 2786−2791.

(28) Amani, M.; Chin, M. L.; Mazzoni, A. L.; Burke, R. A.; Najmaei, S.; Ajayan, P. M.; Lou, J.; Dubey, M. Growth-Substrate Induced Performance Degradation in Chemically Synthesized Monolayer MoS_2 Field Effect Transistors. *Appl. Phys. Lett.* **2014**, *104*, 203506.

(29) Miller, O. D.; Yablonovitch, E.; Kurtz, S. R. Strong Internal and External Luminescence as Solar Cells Approach the Shockley-Queisser Limit. *IEEE J. Photovol.* **2012**, *2*, 303−311.

(30) Lien, D.-H.; Kang, J. S.; Amani, M.; Chen, K.; Tosun, M.; Wang, H.-P.; Roy, T.; Eggleston, M. S.; Wu, M. C.; Dubey, M.; Lee, S.-C.; He, J.-H.; Javey, A. Engineering Light Outcoupling in 2D Materials. *Nano Lett.* **2015**, *15*, 1356−1361.

(31) Liu, Z.; Amani, M.; Najmaei, S.; Xu, Q.; Zou, X.; Zhou, W.; Yu, T.; Qiu, C.; Birdwell, A. G.; Crowne, F. J.; Vajtai, R.; Yakobson, B. I.; Xia, Z.; Dubey, M.; Ajayan, P. M.; Lou, J. Strain and Structure Heterogeneity in MoS_2 Atomic Layers Grown by Chemical Vapour Deposition. *Nat. Commun.* **2014**, *5*, 5246.

(32) Shi, H.; Pan, H.; Zhang, Y.-W.; Yakobson, B. I. Quasiparticle band structures and optical properties of strained monolayer MoS_2 and WS_2. *Phys. Rev. B: Condens. Matter Mater. Phys.* **2013**, *87*, 155304.

(33) Yablonovitch, E.; Gmitter, T. J.; Bhat, R. Inhibited and Enhanced Spontaneous Emission from Optically Thin AlGaAs/GaAs Double Heterostructures. *Phys. Rev. Lett.* **1988**, *61*, 2546−2549.

(34) Richter, A.; Glunz, S. W.; Werner, F.; Schmidt, J.; Cuevas, A. Imprved Quantitative Description of Auger Recombination in Crystalline Silicon. *Phys. Rev. B: Condens. Matter Mater. Phys.* **2012**, *86*, 165202.

(35) Trupke, T.; Zhao, J.; Wang, A.; Corkish, R.; Green, M. A. Very Efficient Light Emission from Bulk Crystalline Silicon. *Appl. Phys. Lett.* **2003**, *82*, 2996−2998.

(36) Hill, H. M.; Rigosi, A. F.; Roquelet, C.; Chernikov, A.; Berkelbach, T. C.; Reichman, D. R.; Hybertsen, M. S.; Brus, L. E.; Heinz, T. F. Observation of Excitonic Rydberg States in Monolayer MoS_2 and WS_2 by Photoluminescence Excitation Spectroscopy. *Nano Lett.* **2015**, *15*, 2992−2997.

(37) Chernikov, A.; Berkelbach, T. C.; Hill, H. M.; Rigosi, A.; Li, Y.; Aslan, O. B.; Reichman, D. R.; Hybertsen, M. S.; Heinz, T. F. Exciton Binding Energy and Non-Hydrogenic Rydberg Series in Monolayer WS_2. *Phys. Rev. Lett.* **2014**, *113*, 076802.

(38) Qiu, H.; Xu, T.; Wang, Z.; Ren, W.; Nan, H.; Ni, Z.; Chen, Q.; Yuan, S.; Miao, F.; Song, F.; Long, G.; Shi, Y.; Sun, L.; Wang, J.; Wang, X. Hopping Transport Through Defect-Induced Localized States in Molybdenum Disulphide. *Nat. Commun.* **2013**, *4*, 2642.

(39) Hong, J.; Hu, Z.; Probert, M.; Li, K.; Lv, D.; Yang, X.; Gu, L.; Mao, N.; Feng, Q.; Xie, L.; Zhang, J.; Wu, D.; Zhang, Z.; Jin, C.; Ji, W.; Zhang, X.; Yuan, J.; Zhang, Z. Exploring Atomic Defects in Molybdenum Disulfide Monolayers. *Nat. Commun.* **2015**, *6*, 6293.

(40) Najmaei, S.; Amani, M.; Chin, M. L.; Liu, Z.; Birdwell, A. G.; O'Regan, T. P.; Ajayan, P. M.; Dubey, M.; Lou, J. Electrical Transport Properties of Polycrystalline Monolayer Molybdenum Disulfide. *ACS Nano* **2014**, *8*, 7930−7937.

(41) Gutierrez, H. R.; Perea-Lopez, N.; Elias, A. L.; Berkdemir, A.; Wang, B.; Lv, R.; Lopez-Urias, F.; Crespi, V. H.; Terrones, H.; Terrones, M. Extraordinary Room-Temperature Photoluminescence in Triangular WS_2 Monolayers. *Nano Lett.* **2013**, *13*, 3447−3454.

G